

RESEARCH ARTICLE

Open Access



# Dynamic spectral characteristics of high-resolution simulated equatorial plasma bubbles

Charles Rino<sup>1\*</sup> , Tatsuhiro Yokoyama<sup>2</sup> and Charles Carrano<sup>1</sup>

## Abstract

Manifestations of severe nighttime equatorial ionospheric disturbances have been observed for decades. It is generally accepted that the phenomena are caused by large depletions, referred to as equatorial plasma bubbles (EPBs), which are initiated on the rising unstable bottom side of the nighttime F layer. Physics-based simulations have enhanced our understanding of the EPB phenomenon. However, until very recently, stochastic structure smaller than  $\sim 10$  km was not well resolved. Recent high-resolution EPB simulations have extended the resolution to hundreds of meters, which provides a unique opportunity to characterize intermediate-scale EPB structure.

This paper presents a summary analysis of simulated high-resolution intermediate-scale EPB structure. Estimation of altitude-dependent power law spectral density function parameters provides an altitude versus time history of the intermediate-scale structure development. Local structure onset is associated with successive bifurcation of rising EPBs. Developed structure characterized by a two-component power law spectral density function ultimately subtends several hundred kilometers in altitude.

Two-component inverse power-law structure was first observed in early in situ rocket measurements. It has been observed in diagnostic measurements of beacon-satellite and GPS scintillation data as well as in situ measurements from Atmospheric Explorer and C/NOFS satellites. The EPB simulation data fully support the reported EPB diagnostics as well as a correlation between the turbulent strength and the large-scale spectral index parameter estimates. However, recent analyses have shown that the correlation is an intrinsic property of power-law parameter estimation.

**Keywords:** Equatorial spread F, Power-law ionospheric structure, Convective plasma instability, Structure characterization

## Introduction

The terminology equatorial spread F (ESF), plumes, and equatorial plasma bubbles (EPBs) evolved, respectively, from ionospheric sounder, coherent radar backscatter, and diagnostic measurements. In situ and remote EPB radio-propagation diagnostics are formally time series generated by the motion of the probe or the interrogating propagation path. Interpreting such diagnostic measurements is challenging because altitude, magnetic field, and temporal structure variations are invariably intermingled. Moreover, time-to-space conversion depends on an unknown structure drift. The dependence of propagation

diagnostics on path-integrated structure further complicates the interpretation of diagnostic measurements.

Physics-based simulations provide an exceptional opportunity to generate definitive structure development measurements. Although the underlying physics has been well established for decades, simulating the generation and dissipation of steep gradients that evolve in unstable regions has, until very recently, limited the resolution that could be achieved to kilometer scales. Recently, simulations that exploit advanced computational capabilities have resolved EPB structure to hundreds of meters.

## Methods/Experimental

High-resolution simulations described in a survey paper by Yokoyama (2017) were made available for the EPB structure analysis presented in this paper. Yokoyama (2017)

\*Correspondence: [charles.rino@bc.edu](mailto:charles.rino@bc.edu)

<sup>1</sup>Institute for Scientific Research, Boston College, 140 Commonwealth Ave., Chestnut Hill, MA 02467, USA

Full list of author information is available at the end of the article

also reviewed the historical development of EPB simulations, which were introduced in the early 1980s. To make the EPB simulations as representative of real-world conditions as possible, multiple EPBs were initiated with an eastward  $E \times B$  drift. The number of EPBs initiated depends on the initial conditions. However, the simulation analyzed in this paper shows that intermingling of structure from multiple EPBs populates extended structure regions.

The conditions under which EPBs develop and how the large-scale structure evolution can be reconciled with diagnostic measurements, particularly the coherent-backscatter radar echoes that delineate the plumes, have been studied extensively (Hysell 2000). Less attention has been given to characterizing intermediate-scale stochastic structure from tens of kilometers to hundreds of meters. Figure 1 is a perspective view of the developed EPB structure. The left frame shows the central meridian plane slice, which emphasizes smoothly varying field-aligned structure. The right frame shows vertical and horizontal slice planes, which emphasize stochastic cross-field structure.

Stochastic structure is definitively reproduced only in slice planes that cut across field lines. For this study, evolving structure from the equatorial slice plane and two offset slice planes, identified by the rays in Fig. 2, were extracted from the three-dimensional simulations. The electron density variation in Fig. 2 shows that field-aligned structure intercepts systematically varying background electron density. The offset slice planes allow exploration of the field-aligned structure translation.

The left frame in Fig. 3 shows developed equatorial-plane structure detail 1 h after initiation. Seeded bottom-side perturbations initiated five EPBs that evolved at different rates depending on their zonal location at initiation. Slice planes were sampled uniformly from 300 to 800 km with 1120 zonal samples at 333.56 m and 1821 vertical samples at 700.83 m. The right frame shows the zonal average electron density (blue) with an overlaid smoothed profile (red). Figures 4 and 5 show the offset1 and offset2 structure summaries. The structure flux tubes intercept the offset planes at progressively lower altitudes. The structure in the offset2 slice plane is mapped below the 300 km lower limit.

The zonal average electron densities shown in the right frames of Figs. 3, 4, and 5 are proportional to zonal path-integrated total electron content (TEC), which can be measured with navigation satellite transmissions received by low orbiting satellite occultations (Tsai et al. 2011). Although such measurements do not resolve the intermediate-scale structure directly, scintillation of the probing signals can be processed for structure diagnostics.

To summarize the structure evolution, the slice frames were cyclically shifted to compensate for the 120 mps eastward drift. Periodic simulation boundary conditions confined the zonal extent of the realizations. The residual formed by subtracting the smoothed average profiles provides a measure of the height-dependent structure development. The time resolution for the EPB simulations is 0.1 s but reported at 10 s intervals. Figure 6 summarizes the evolution of the structure residuals at 100 s

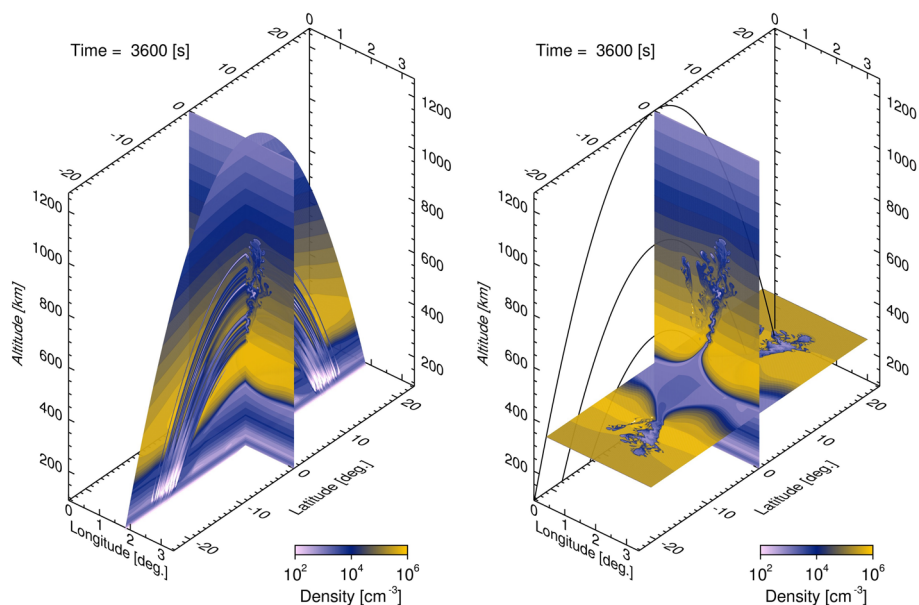


**Fig. 1** Perspective view of the EPB simulation environment. The left frame shows the central meridian plane. The right frame shows the structure in two orthogonal slice planes

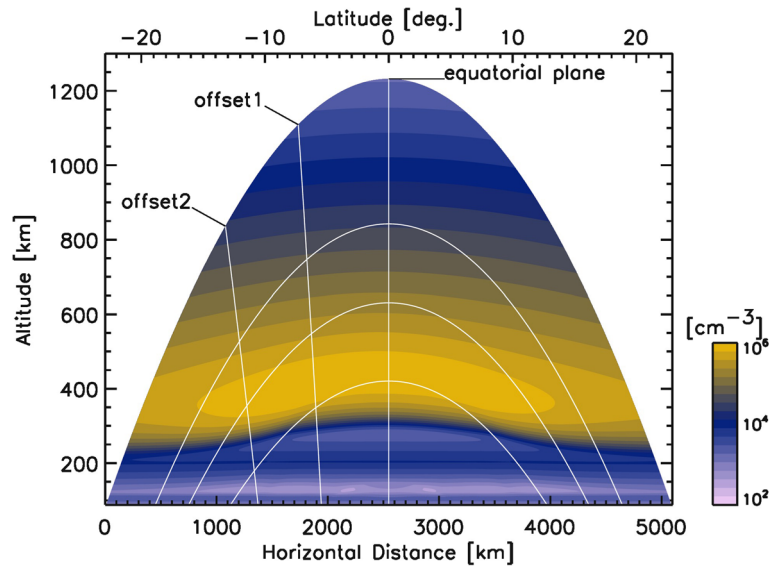


**Fig. 2** Meridian slice plane with overlaid rays locating vertical equatorial slice plane and two offset slice planes excised for structure analysis

intervals. Structure onset can be identified at a specific time and altitude, which is the point where the highest EPB penetrates the F-region peak electron density.

To explore the structure onset detail, Fig. 7 shows four consecutive 10 s zoomed images of the most rapidly progressing central EPB. The steepening gradient at the head of the EPB generates local depletions flanked by

enhancements, which are referred to as bifurcations. Each bifurcation initiates a secondary bifurcation. The process of successive bifurcation creates a fractal-like structure cascade. The progression in Fig. 4 shows that once initiated, successive bifurcation proceeds very rapidly. A more detailed discussion can be found in Yokoyama et al. (2014).

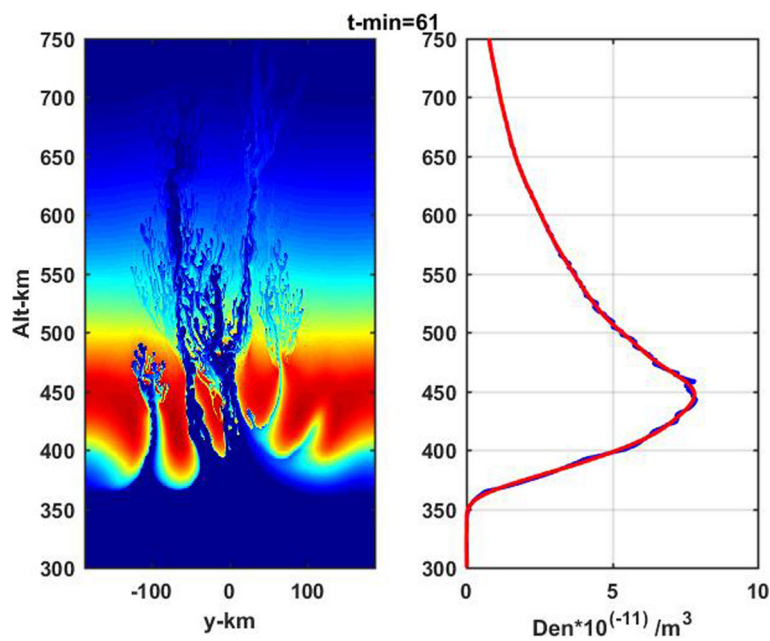


**Fig. 3** The left frame shows the equatorial plane structure at 1 h. The right frame shows the path-integrated density (blue) with a smoothed profile overlaid (red)

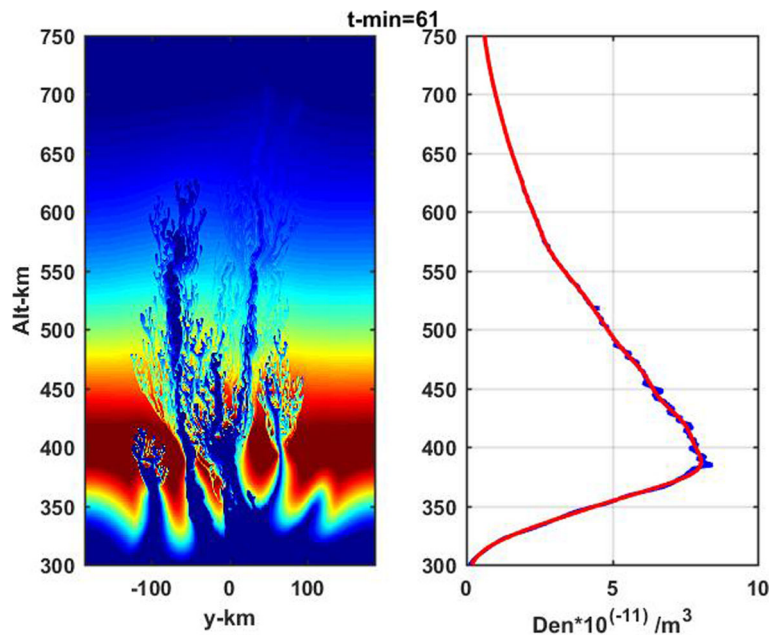


**Fig. 4** The left frame shows the offset1 plane structure at 1 h. The right frame shows the path-integrated density (blue) with a smoothed profile overlaid (red)

### Structure characterization

EPB electron density slice-plane realizations are formally two-dimensional scalar fields,  $N_e(y, z)$ , where  $y$  and  $z$  represent cross-field and altitude, respectively. Assuming that  $N_e(y, z)$  is statistically homogeneous, the stochastic structure can be characterized by a two-dimensional spectral density function (SDF),

which is formally the expectation of the intensity of two-dimensional Fourier decompositions of  $N_e(y, z)$  realizations.

### Power-law models

Published in situ measurements and remote diagnostics imply an underlying two-component power-law

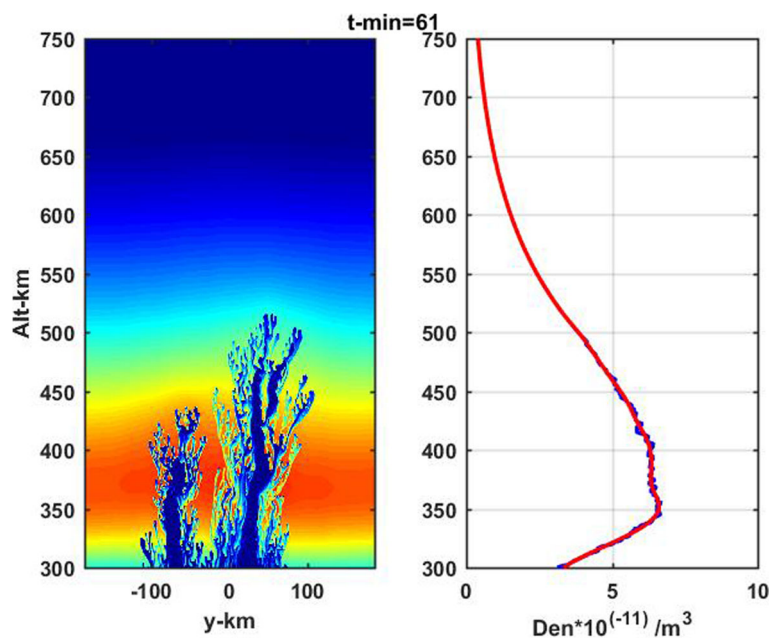


**Fig. 5** The left frame shows the offset2 plane structure at 1 h. The right frame shows the path-integrated density (blue) with a smoothed profile overlaid (red)

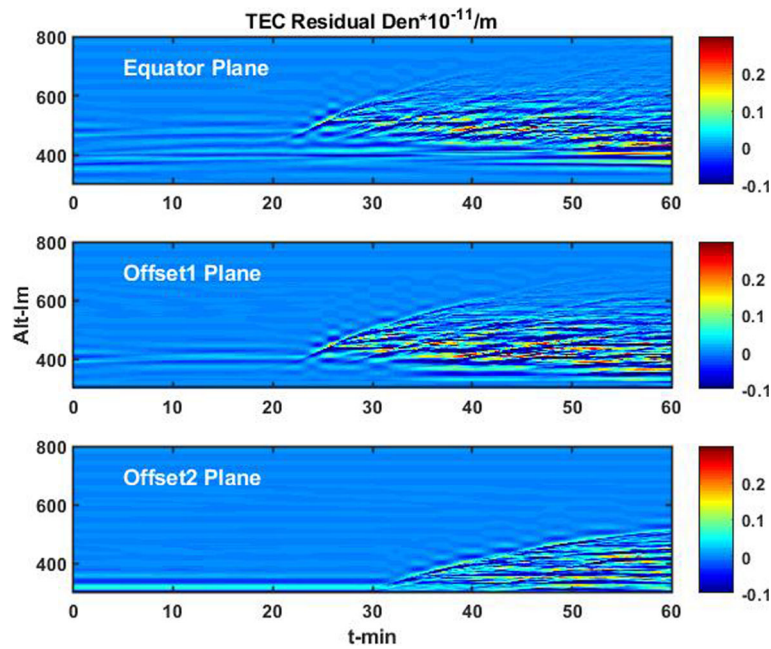


**Fig. 6** Evolution of height-dependent residual structure at 100 s for equatorial, offset1, and offset 2 slices

SDE. The following analytic representation is introduced to guide structure characterization:

$$\Phi_{N_e}(q) = C_s \begin{cases} q^{-p_1} & \text{for } q \leq q_0 \\ q_0^{p_2-p_1} q^{-p_2} & \text{for } q > q_0 \end{cases}, \quad (1)$$

where

$$q = \sqrt{q_y^2 + \beta q_z^2}, \quad (2)$$

is the magnitude of the spatial frequency vector  $[q_y, q_z]$  in radians per meter. The  $\beta$  coefficient accommodates

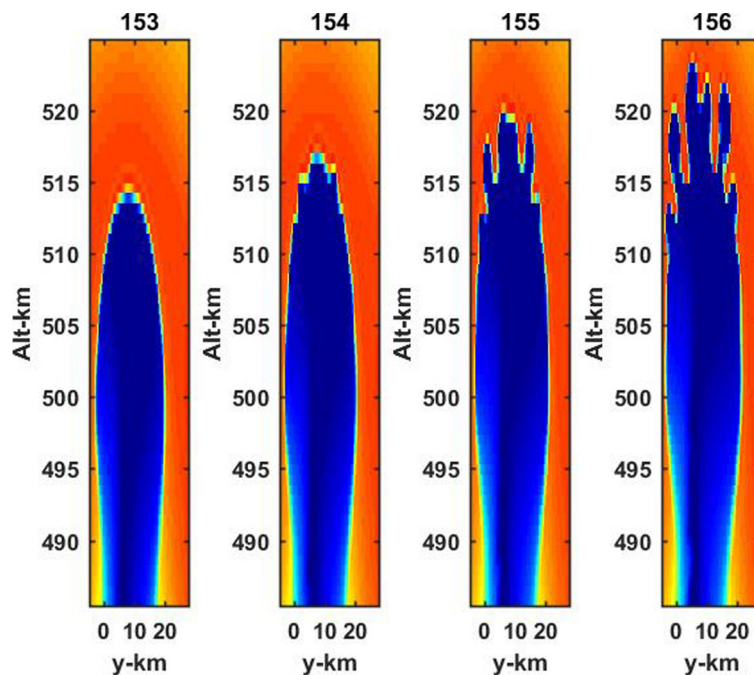


**Fig. 7** Numbered frames show zoomed views at 10 s intervals of the central EPB that generated the structure shown in Fig. 3

projection of the radial variation of field-aligned structure. The defining parameters are turbulent strength,  $C_s$ ; the break frequency,  $q_0$ ; and the spectral indices,  $p_n$  corresponding to subranges of spatial frequencies smaller than ( $n = 1$ ) and larger than ( $n = 2$ )  $q_0$ .

In situ measurements are one-dimensional scans. If the structure volume were stochastic in all three dimensions, the measured one-dimensional SDF would be represented by a two-dimensional integration of the three-dimensional SDF. For field-aligned two-dimensional stochastic structures a slice plane containing the one-dimensional scan must be constructed. Configuration-space realizations populate arbitrarily oriented slice planes for extrapolation (Rino et al. 2018). For the EPB analysis, the cross-field orientation of the slice planes were selected for direct structure measurement. One-dimensional SDFs are related to (1) by the integration

$$\Phi_{N_e}^1(q) = \int_{-\infty}^{\infty} \Phi_{N_e}(q_y, q_z) \frac{dq_z}{2\pi}. \quad (3)$$

For (3) to be well defined, the power-law variation must be specified in more detail. In the EPB realizations, there is a transition from stochastic to trend-like variation at small spatial frequencies. At sufficiently high frequencies, the physics supporting the EPB simulations is incomplete. Furthermore, as already noted, the stochastic structure itself varies with altitude. To capture these details, the following height-dependent one-dimensional SDF *hypothesized* for EPB structure characterization:

$$\Phi_{N_e}(q) = C_s \begin{cases} q^{-\eta_1} & \text{for } q \leq q_0 \\ q_0^{\eta_2 - \eta_1} q^{-\eta_2} & \text{for } q > q_0 \end{cases}. \quad (4)$$

The one-dimensional model captures a broad range of structure characteristics as defined by the turbulent strength  $C_s$ , the spectral indices  $\eta_n$ , and the break frequency  $q_0$ . For example, if  $\eta_1 \simeq 0$ ,  $q_0$  can be interpreted as an outer scale. If  $\eta_1 \simeq \eta_2$ , the SDF is a single power law. Generally,  $\eta_1 \leq \eta_2$ . However, enhanced low-frequency structure might lead to the opposite ordering,  $\eta_1 > \eta_2$ . In all cases, the variation of  $C_s$  provides a measure of overall structure intensity.

Establishing the relation between  $\eta_n$  and  $p_n$ , which is nominally  $\eta_n = p_n - 1$ , is beyond the scope of this study. However, ionospheric structure models can be validated by comparing predicted height-dependent one-dimensional structure characteristics with the measured EPB structure.

### Irregularity parameter estimation

Irregularity parameter estimation (IPE) systematically adjusts the defining parameters to minimize a measure of the disparity between an SDF estimate and the theoretical SDF. An IPE procedure for estimating scintillation intensity SDF parameters was introduced by Carrano and Rino

(2016). The original IPE procedure was refined to maximize the likelihood that the periodogram was derived from a realization with the theoretical SDF (Carrano et al. 2017). For characterizing the EPB SDFs, the maximum likelihood estimation (MLE) procedure was adapted for power-law SDF estimation as described in Rino and Carrano (2018). Power-law parameter estimation is more challenging than intensity scintillation parameter estimation because of the singular behavior of unmodified power-law SDFs at zero frequency.

The MLE SDF estimate is the average of  $M$  periodograms, formally

$$\widehat{\Phi}_{N_e} = \frac{1}{M} \sum_{l=1}^M \widehat{\Phi}_n^{(l)}, \quad (5)$$

where the periodogram is defined as

$$\widehat{\Phi}_n^{(l)} = \frac{\Delta y}{N} \left| \sum_{k=0}^{N-1} N_e^{(l)}(k\Delta y) \exp\{-ink/N\} \right|^2. \quad (6)$$

The index  $n$  corresponds to the spatial frequencies

$$2\pi/(N\Delta y) \leq n\Delta q \leq 2\pi/\Delta y, \quad (7)$$

where  $\Delta y$  is the  $y$  sample interval, and  $\Delta q = 2\pi/(N\Delta y)$  is the spatial-frequency resolution. The index  $l$  identifies the altitude at which the zonal scan is extracted. One can show that

$$\langle \widehat{\Phi}_{N_e} \rangle = \Phi_{N_e} \quad (8)$$

MLE exploits the fact that the probability distribution function (PDF) of the periodogram is well approximated by a  $\chi$  distribution with 2 degrees of freedom. The  $\chi$  distribution with  $2M$  degrees of freedom follows for the summation.

It is well known that periodogram estimates are contaminated by the sidelobes of end-point discontinuities. Moreover, efficient discrete Fourier transformation (DFT) evaluation requires  $N$  to be even with as many factors as possible, ideally a power of 2. The Welch method (Welch 1995) uses windowing and segmentation with averaging. Periodogram variants, such as maximum entropy estimates (Fougere 2009), provide additional variants. However, MLE relies on unbiased spectral estimates with  $\chi$  distributions, whereby it is desirable to stay as close to (6) as possible. After some exploration, it was found that using the full 373.6 km  $y$  extent of the data zero extended to a *nice* FFT number gave the best results. Following (Rino and Carrano 2018), periodograms from two altitudes ( $M = 2$ ) were averaged.

Multi-parameter MLE used a MATLAB implementation of the Nelder-Mead simplex algorithm (Olsen and Nelsen 1975). The procedure is surprisingly robust in that fits were made to quasi-deterministic SDFs with no stochastic structure as well SDFs from realizations with

fully developed stochastic structure. The two classes are readily distinguished by the reported IPE parameters.

**Results**

MLE-IPE with  $M = 2$  was performed over each set of slice-plane scans. Figures 8, 9, and 10 summarize the parameter estimates. The periodogram sample interval is twice the height sampling (1.4 km). The  $C_s > 200$  estimates shown in the upper frames of Figs. 8, 9, and 10 capture the unstructured regions identified in Fig. 6. From the second and third frames in Figs. 8, 9, and 10, we see that  $\eta_1 < \eta_2$  within the unstructured regions. Outside the structured regions, the pattern is reversed. For ease of interpretation,  $\sigma_b = 2\pi/q_0$  is reported rather than the break frequency.

Figure 11 compares representative equatorial slice-plane SDFs extracted from the unstructured (upper frame) and structured (lower frame) altitude ranges. The smoothly varying structure generates enhanced structure at the lower spatial frequencies with sidelobes populating the higher frequencies. The MLE-IPE parameters capture the SDF envelope with  $\eta_1 > \eta_2$  and a break frequency scale near 5 km. The developed structure populates the lower frequencies more uniformly with a more rapid decrease at higher frequencies. MLE-IPE captures the structure with  $\eta_1 < \eta_2$  and larger  $C_s$  values. The transition from unstructured to structured SDFs necessarily includes SDFs with  $\eta_1 \approx \eta_2$ .

The break scale estimates within the structured region as summarized in the lower frames of Figs. 8, 9, and 10

show more variability. Movie presentations of slice plane realizations and the associated SDFs highlight the intermingling of the large-scale EPB structure with the background. The several kilometer size of the bifurcations shown in Fig. 7 appears to be a lower bound on the break frequency. However, the intermingling of the EPBs with the background evidently modulates the structure.

**Discussion**

The simulations reveal abrupt structure onset as a transition from quasi-deterministic structure with a steep low-frequency power-law index to the more representative two-component SDF structure with  $\eta_1 < \eta_2$ . To the extent that field lines mapped from the equatorial plane are captured in the offset planes, the structure characteristics are nearly identical.

To summarize the stochastic structure characteristics, Figs. 12, 13, and 14 show probability distributions of the structure with  $C_{sdB} > 200$  dB. The developed structure is fairly uniform. The  $\eta_1$  and  $\eta_2$  distributions show peaks just below 1.5 and just above 2.5. These values are consistent with the C/NOFS results reported by Rino et. al (2016). They are also consistent with the parameters Retterer (2010) used in the PBMOD ionospheric scintillation model, with allowance for the relation  $p_n = \eta_n + 1$ . Moreover, EPB  $C_s$  range is comparable to the reported C/NOFS values when the unscaled C/NOFS values are translated to common electron density units.

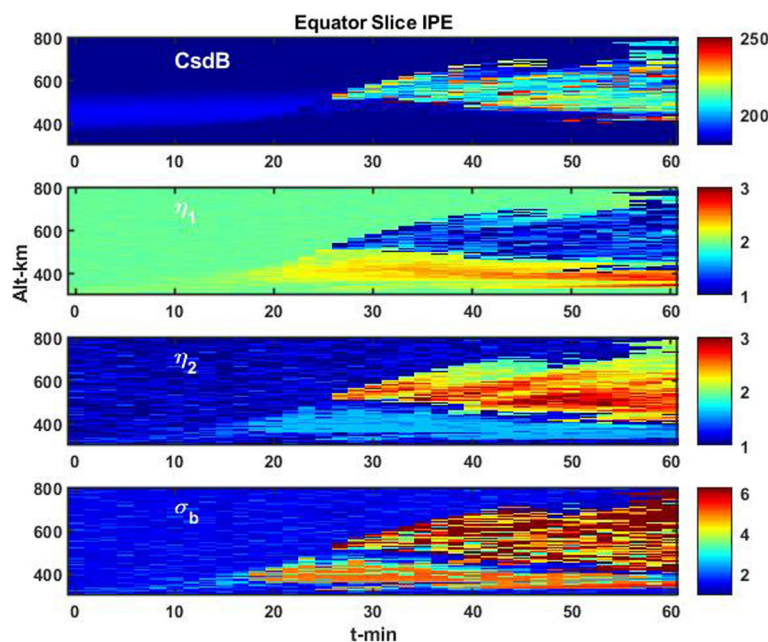


**Fig. 8** MLE-IPE SDF parameter estimates from equatorial slice plane realizations at 100 s, where  $\sigma_b = 2\pi/q_0$

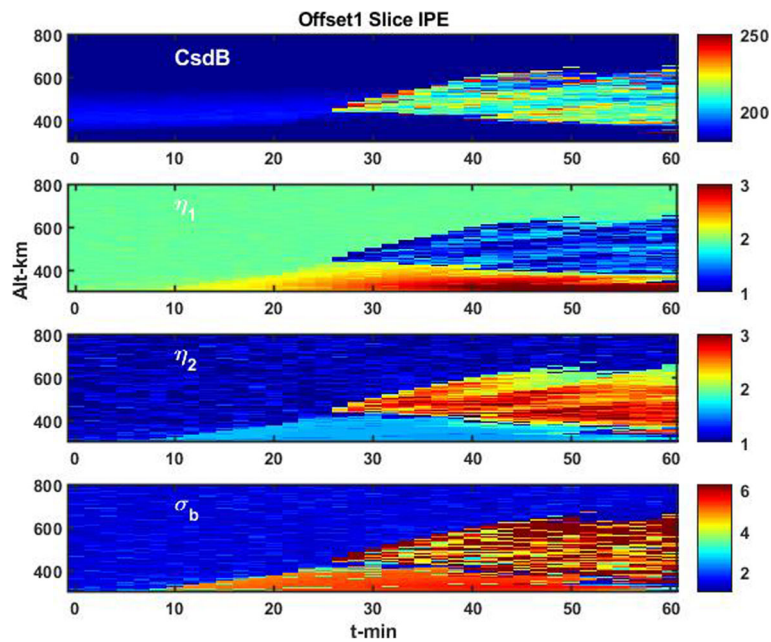


**Fig. 9** MLE-IPE SDF parameter estimates from offset1 slice plane realizations at 100 s, where  $\sigma_b = 2\pi/q_0$

The C/NOFS break scales reported by Rino et. al (2016) are smaller than the break scales from the EPB analysis. One possibility is the resolution of wavelet scale spectra used for the C/NOFS analysis. Alternatively, as noted in the previous section, the EPB break scale is evolving and sensitive to the background structure. Precise

measurement of the initiation and evolution of the break scale is a topic for targeted special study.

Transition populations with  $\eta_1 \simeq \eta_2$  are very small. However, the simulated background structure is idealized and might not represent real-world background structure. Bhattacharyya et al. (2003) showed that the latitudinal

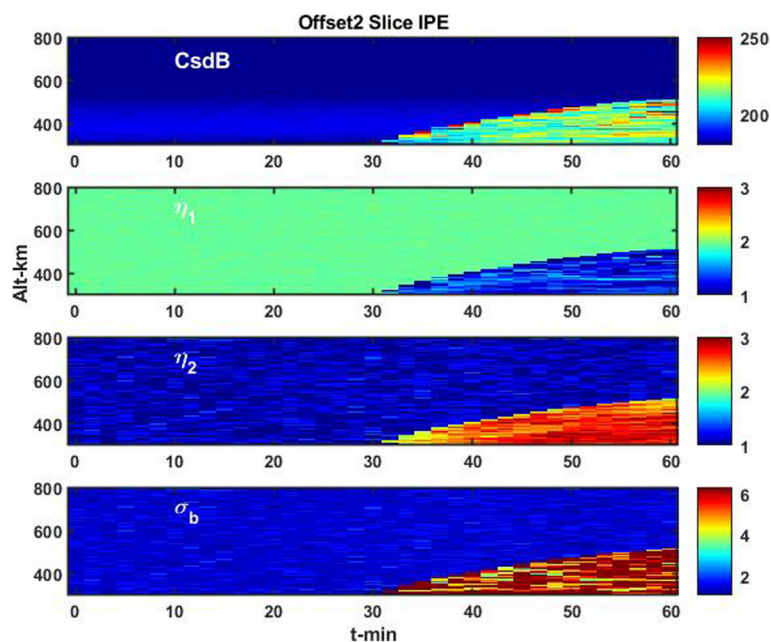


**Fig. 10** MLE-IPE SDF parameter estimates from offset2 slice plane realizations at 100 s, where  $\sigma_b = 2\pi/q_0$

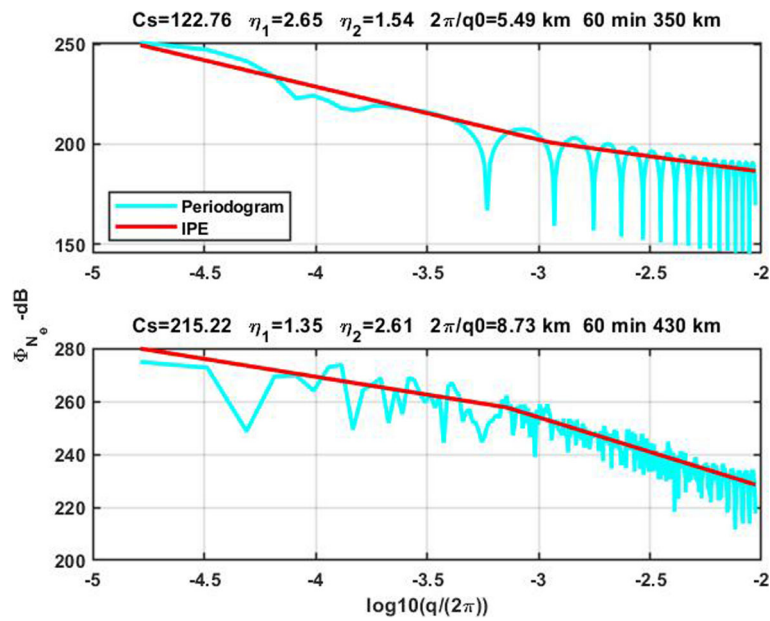


**Fig. 11** SDFs (magenta) with overlaid theoretical SDFs from IPE parameters (red)

dependence of EPB structure can be explained by invoking a single power-law structure in the lower F-region, with attendant smaller scintillation levels.

The offset1 and offset2 PDFs shown in the lower frames of Figs. 13 and 14 have peaks between 4 and 5 km, which is consistent with the dimensions of the initial bifurcations shown in Fig. 7. The distribution of larger break scales is associated with the aforementioned

intermingling of background structure. The offset2 structure is fully contained in the enhanced background, which would explain the enhanced distribution of larger break scales.

Figure 15 shows a scatter diagram of the measured EPB parameters  $Cs_{dB}$  versus  $\eta_1$ . The correlation is identical to the correlation reported in Rino et al. (2016) from an analysis of 4 years of C/NOFS data. The overlaid log-linear

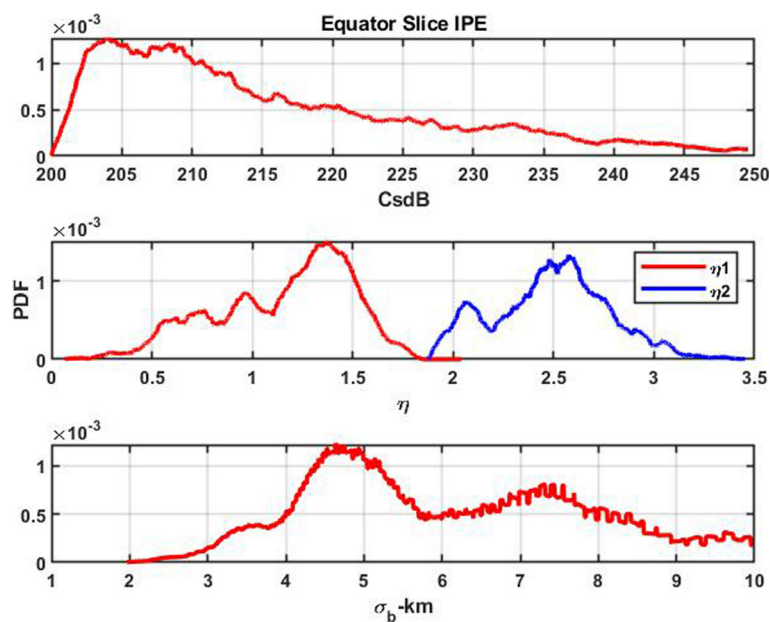


**Fig. 12** Probability distributions of equatorial plane stochastic structure

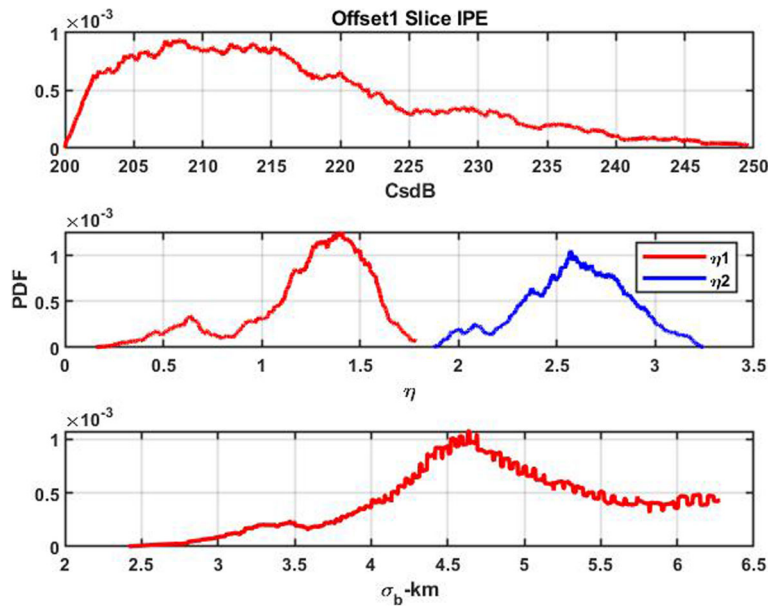


**Fig. 13** Probability distributions of offset1 plane stochastic structure

dependence has the reported slope of 0.02 nepers per dB of  $C_s$  change. The tendency for the correlation to appear in narrow bands was also noted in the C/NOFS data. However, we now know from the analysis reported by Rino and Carrano (2018) that the correlation can be completely explained as an intrinsic property of power-law irregularity parameter estimation. The correlation occurs because the  $\chi$  distribution with small degrees of freedom generates a

significant population of errors larger than the mean. This is reflected in the  $C_s$  distributions shown in the upper frames of Figs. 12, 13, and 14, which favor larger  $C_s$  values.

As a consequence of the correlation, the true values of  $C_s$  and  $\eta_1$  are likely to be closer to the central values in Fig. 15. As a test of this effect, the equatorial MLE-IPE was recomputed with  $M = 10$ , which reduces the altitude resolution to 7 km. Figure 16 shows the

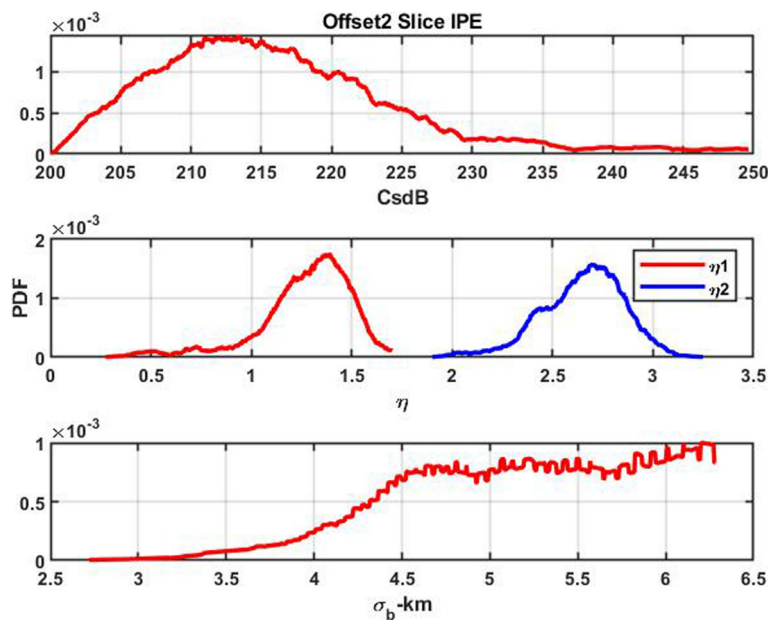


**Fig. 14** Probability distributions of offset2 plane stochastic structure

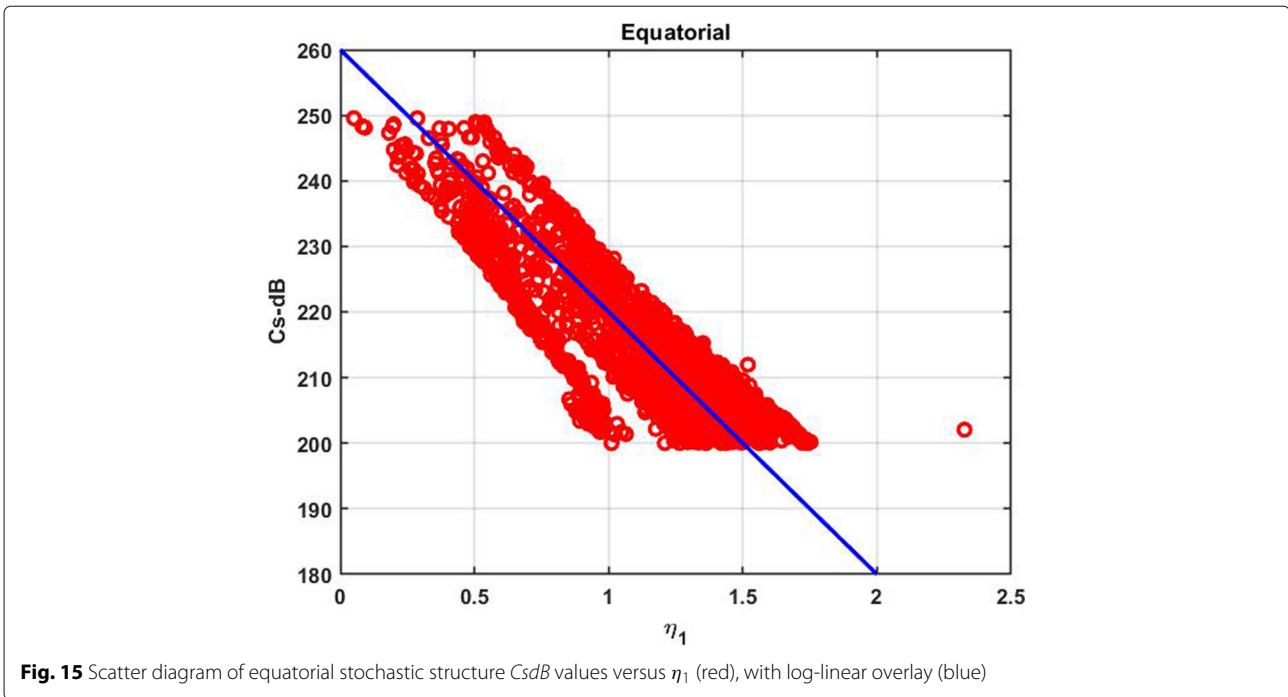


**Fig. 15** Scatter diagram of equatorial stochastic structure  $CsdB$  values versus  $\eta_1$  (red), with log-linear overlay (blue)

probability distributions. The  $M = 10$  equatorial  $C_s$  distribution is more concentrated between 210 and 215 dB. The  $\eta_1$  and  $\eta_2$  peaks are sharpened somewhat, while larger scales dominate the break frequency scale. Because resolution requires larger segments, which reduces the number of segments that can be averaged, trades between resolution and statistical uncertainty are unavoidable.

However, the variability of the break scale appears to convey information about the underlying structure. These are clearly topics for further study.

**Conclusions**

The analysis of high-resolution EPB simulations presented in this paper supports that generally accepted hypothesis

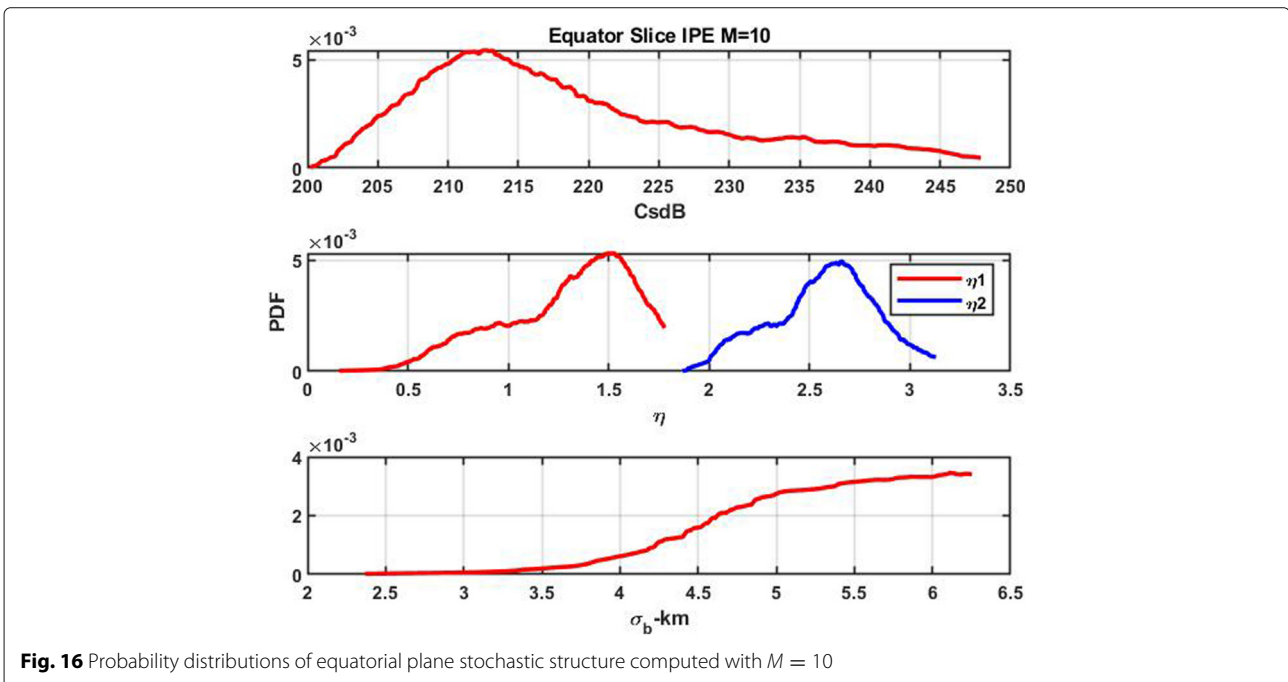


**Fig. 16** Probability distributions of equatorial plane stochastic structure computed with  $M = 10$

that developed EPB structure can be characterized by a one-dimensional two-component power-law SDF with  $\eta_1$  somewhat smaller than 1.5 and  $\eta_2$  somewhat larger than 2.5. The scale associated with the break frequency varies from the 4 to 5 km bifurcation scale to much larger values reflecting intermingling of the EPB structure with the F-region background. In units of electrons per cubic centimeter, the decibel turbulent strength parameter falls between 210 and 215 dB. A persistent correlation between the measured turbulent strength and the large-scale spectral index is an intrinsic property of power-law parameter estimation that researchers need to be aware of. Structure evolving in the equatorial plane maps along field lines with no significant structure variation. However, structure mapped below F-layer was not investigated.

The transition from smoothly varying background structure to stochastic structure is manifest by an SDF transition initially reflecting large-scale structure with  $\eta_1 > \eta_2$  to developed structure with  $\eta_1 < \eta_2$ . The transition through a single power law with  $\eta_2 \simeq \eta_1$  is not a prominent feature, but we have argued that a smooth background is idealized and not representative of real ionospheric structure. Within the structured region, the structure is uniform over the 30 min interval with developed structure and over an altitude range of several hundred kilometers. The result favors the standard interpretation that two-dimensional SDF characterizing the cross-field structure has the two-dimensional form (1) with  $p_n = \eta_n + 1$ .

We conclude by recalling that the 1971 PLUMEX campaign successfully launched a powerful rocket into an EPB being tracked by coherent-scatter radar. The rocket carried a radio beacon and a Langmuir probe. Analysis of the PLUMEX radio-beacon and Langmuir probe data summarized by Rino et al. (1981) showed the first evidence of a two-component power-law structure. Numerical simulations being developed by the U. S. Naval Research Laboratory and reviewed by Yokoyama (2017) were being used to interpret the PLUMEX results. To quote the final sentence in the PLUMEX paper: *Rapid progress is being made in such [numerical simulations], and we believe that the simulations have the potential to verify the results presented in [the PLUMEX] paper.*

#### Abbreviations

EPB: Equatorial plasma bubble; PSD: Power spectral density; SDF: Spectral density function

#### Acknowledgements

The computation was performed on the FX100 supercomputer system at the Information Technology Center, Nagoya University, and Hitachi SR16000/M1 system at NICT, Japan.

#### Funding

This work was supported by JSPS KAKENHI Grant Number JP16K17814. This work was also supported by the computational joint research program of the

Institute for Space-Earth Environmental Research (ISEE), Nagoya University, Japan.

Support for CR and CC was provided under Advanced Data Driven Specification and Forecast Models for the Ionosphere-Thermosphere System, Air Force Contract FA9453-12-C-0205

#### Availability of data and materials

The simulation data are stored on the FX100 supercomputer system at the Information Technology Center, Nagoya University, and Hitachi SR16000/M1 system at NICT, Japan. TY (tyoko@nict.go.jp) can provide data upon request.

#### Authors' contributions

All of the simulations analyzed in this paper were performed by TY and generously reformatted and made available to CR who performed the analysis. The analysis was conceived by CR and TY at the December 2016 AGU meeting following a presentation by TY. CC has worked extensively to improve scintillation diagnostics, particularly definitive SDF parameter estimation, which was central to this study. All authors read and approved the final manuscript.

#### Competing interests

The authors declare that they have no competing interest.

#### Publisher's Note

Springer Nature remains neutral with regard to jurisdictional claims in published maps and institutional affiliations.

#### Author details

<sup>1</sup>Institute for Scientific Research, Boston College, 140 Commonwealth Ave., Chestnut Hill, MA 02467, USA. <sup>2</sup>National Institute of Information and Communications Technology, 4-2-1 Nukui-Kitamachi, Koganei, Tokyo 184-8795, Japan.

Received: 27 August 2018 Accepted: 16 November 2018

Published online: 13 December 2018

#### References

- Bhattacharyya A, Groves KM, Basu S, Kuenzler H, Valladares CE, Sheehan R (2003) L-band scintillation activity and space-time structure of low-latitude UHF scintillations. *Radio Sci* 38(1):1004. <https://doi.org/10.1029/2002RS002711>
- Carrano CS, Rino CL (2016) A theory of scintillation for two-component power law irregularity spectra: overview and numerical results. *Radio Sci* 51:789–813. <https://doi.org/10.1002/2015RS005903>
- Carrano CS, Rino CL, Groves (2017) Maximum likelihood estimation of phase screen parameters from ionospheric scintillation spectra. In: 15th International Ionospheric Effects Symposium. Radio Science Publications, Alexandria, pp 1–11, May 9–11
- Fougere PF (2009) On the accuracy of spectrum analysis of red noise processes using maximum entropy and periodogram methods simulation studies and application to geophysical data. *J Geophys Res* 90(A5):4355–4366
- Hysell DL (2000) An overview and synthesis of plasma irregularities in equatorial spread f. *J Atmos Solar-Terr Phys* 62:1037–1056
- Livingston RC, Rino CL, McClure JP, Hanson WB (1981) Spectral characteristics of medium-scale equatorial F-region irregularities. *J Geophys Res* 86:7421–7428
- Olsen DM, Nelsen LS (1975) The Nelder-Mead simplex procedure for function minimization. *Technometrics* 17(1):46–51
- Retterer JM (2010) Forecasting low latitude radio scintillation with 3-D ionospheric plume models: 2. scintillation calculation. *J Geophys Res* 115. <https://doi.org/10.1029/2008JA013840>
- Rino CL, Tsunoda RT, Petriccks, Livingston RC, Kelley MC, Baker DK (1981) Simultaneous rocket-borne beacon and in situ measurements of equatorial spread F–intermediate wavelength results. *J Geophys Res* 84(A4):2411–2420
- Rino CL, Groves KM, Carrano CS, Roddy PA (2016) A characterization of intermediate-scale spread F structure from four years of high-resolution C/NOFS satellite data. *Radio Sci* 51. <https://doi.org/10.1002/2015RS005841>
- Rino C, Carrano C (2018) On the characterization of intermediate scale ionospheric structure. *Radio Sci*. Accepted for publication
- Rino C, Carrano C, Groves K, Yokoyama T (2018) A configuration space model for intermediate scale ionospheric structure. *Radio Science*. <https://doi.org/10.1029/2018RS006678>

- Tsai L-C, Cheng K-C, Liu CH (2011) GPS radio occultation measurements on ionospheric electron density from low earth orbit. *J Geodesy* 85:7421–7428
- Welch P (1995) The use of fast fourier transform for the estimation of power spectra: a method based on time averaging over short, modified periodograms. *IEEE Trans Audio Electroacoustics* 15(2):70–73
- Yokoyama T, H, Shinagawa H, Jin H (2014) Nonlinear growth, bifurcation, and pinching of equatorial plasma bubble simulated by three-dimensional high-resolution bubble model. *J Geophys Res Space* 119:10474–10482. <https://doi.org/10.1002/2014JA020708>
- Yokoyama T (2017) A review on the numerical simulation of equatorial plasma bubbles toward scintillation evaluation and forecasting. *Prog Earth Planet Sci* 4:37. <https://doi.org/10.1186/s40645-017-0153-6>

**Submit your manuscript to a SpringerOpen<sup>®</sup> journal and benefit from:**

- ▶ Convenient online submission
- ▶ Rigorous peer review
- ▶ Open access: articles freely available online
- ▶ High visibility within the field
- ▶ Retaining the copyright to your article

---

Submit your next manuscript at ▶ [springeropen.com](http://springeropen.com)

---